Amine-Functionalized Fe_2O_3-SiO_2 Core-Shell Nanoparticles with Tunable Sizes

Yun Teng, Chengpeng Jiang, *Student Member*, *IEEE*, Antonio Ruotolo, *Senior Member*, *IEEE*, Philip W. T. Pong, *Senior Member*, *IEEE*

***Abstract*—Iron oxide magnetic nanoparticles (MNPs) coated with uniform silica shell were synthesized through thermal decomposition and inverse microemulsion methods. The iron oxide MNPs were further coated with silica shells through hydrolysis reaction. For the resulting core-shell MNPs, size regulation of both the magnetic core and the porous shell were achieved, enabling the modulation of their magnetic properties and magnetic interactions. Core-shell MNPs were finally functionalized with amine groups, and immobilized on gold surface due to charge-neutral amine/gold interactions. It was observed that the immobilization process was enhanced under external magnetic field.**

***Index Terms*— Magnetic nanoparticle, Core-shell nanoparticle, Nanoparticle size control, Nanoparticle functionalization.**

I. Introduction

IRON oxide magnetic nanoparticles (MNPs) have attracted increasing attentions and exhibit great potential for biomedical applications due to their chemical stability, excellent biodegradability and high saturation magnetization [1]–[3]. The properties of iron oxide MNPs including particle size, particle shape, and surface chemistry are closely related to their synthesis route [4]. Over the past decade, several methods have been developed to synthesize iron oxide MNPs [5]–[7]. Among them, thermal decomposition in organic phase is an excellent method to obtain iron oxide MNPs with uniform shape and size, although the synthesized MNPs are hydrophobic and not suitable for direct use towards biomedical applications [8]–[10].

Surface modification of iron oxide MNPs is highly required to transfer them into aqueous media and prevent particle aggregation. Silica coating is a promising solution due to its mesoporous structure, biocompatibility and easy conjugation with various functional groups, which can be further utilized for biomedical sensing and labeling [11]–[14]. Currently, silica coating of iron oxide MNPs can be performed through two prevailing routes, namely Stöber method and inverse microemulsion method [11], [15]. The Stöber method cannot be applied for the MNPs which are insoluble in polar media [16]. The inverse microemulsion method has been extensively explored due to its ability of silica coating for MNPs dispersed in organic phase [17]. The unique core-shell structure with magnetic core encapsulated by mesoporous silica shell hold much promise for targeted drug delivery, bio-separation, bio-conjugation, surface immobilization, and diagnostic analysis [18]–[20]. To achieve practical applications, the silica-coated iron oxide MNPs were usually functionalized by specific chemical species for realizing the conjugation between the silica surface and the desired biomolecule such as enzymes, antibodies, DNAs, or other coupling agents [12], [21]. The resulting functionalized core-shell MNPs makes them ideal candidates for protein absorption and separation, cell imaging and labeling, and surface immobilization [22], [23]. Generally, the silica surface can be functionalized with common functional groups including phenyl groups, amine groups, aliphatic hydrocarbons, and thiol ligands [24]–[27]. Herein, we specifically focus on functionalizing the silica-coated iron oxide MNPs with amine groups, because the primary amines can react with the carboxyl groups in various proteins and molecules for conjugation and immobilization [28].

For the silica-coated iron oxide MNPs, the size and distribution of the magnetic core greatly influence their size-dependent magnetic properties [4], [29]. Especially, when particle size decreases to a certain value in the sub-20 nm regime, iron oxide MNPs demonstrate superparamagnetic behavior, which means they can respond to an external magnetic field without acquiring permanent magnetic moments [30]. On the other hand, the thickness of the mesoporous shell is closely related to the surface-to-volume ratio and magnetic interactions of the core-shell MNPs [31]. Thus, it is critical to control the core diameter and the shell thickness respectively, while maintaining the core-shell structure. Several research groups working on this topic have studied the influence of surfactant and TEOS on silica shell formation, though their products sometimes suffered from issues such as free-core or multi-core [13], [16]. Besides, achievements in improving the uniformity and controlling the thickness of silica coating have been realized in previous research works [14], [32]. However,

Manuscript received July 10, 2016; revised October 25, 2016; accepted November 28, 2016. This work was supported by Seed Funding Program for Basic Research, Seed Funding Program for Applied Research and Small Project Funding Program from HKU, ITF Tier 3 funding (ITS-104/13, ITS-214/14), and University Grants Committee of HK (AoE/P-04/08).

Y. Teng, C. Jiang, and P. W. T. Pong are with the Department of Electrical and Electronic Engineering, University of Hong Kong, Hong Kong (e-mail: ppong@eee.hku.hk).

A. Ruotolo is with the Department of Physics and Materials Science, City University of Hong Kong, Hong Kong.

systematic investigations about the effect of synthesis conditions on core diameter as well as shell thickness, the influence of silica coating on magnetic properties of the core-shell MNPs, and the immobilization of functionalized core-shell MNPs under magnetic field are scarcely reported in literature.

In this work, we report a facile protocol for chemically synthesizing amine-terminated core-shell Fe_2O_3-SiO_2 MNPs with controlled sizes in terms of both the magnetic core and the mesoporous shell. Experimental parameters affecting the core-shell size, including the molar ratio of surfactant to precursor, the amount of solvent, the concentration of MNPs, and the reaction time were analyzed and discussed. Size regulation of both the magnetic core and the porous shell were attempted to change the magnetic properties and magnetic interactions of the core-shell MNPs. Furthermore, surface functionalization was achieved by treating the Fe_2O_3-SiO_2 MNPs with APTES. Finally, immobilization of the functionalized Fe_2O_3-SiO_2 MNPs on gold surface was studied, and the influence of externally applied magnetic field on the immobilization process was investigated.

II. Experimental

A. Materials

Iron(III) oxyhydroxide (FeOOH), oleic acid (90%), and octadecene (90%) were purchased from Aldrich. Polyoxyethylene (10) octylphenyl ether (Triton X-100), aqueous ammonia (25%), tetraethyl orthosilicate (TEOS, 98%), 3-aminopropyl triethoxysilane (APTES, 99%), ethanol, hexanol, chloroform, and cyclohexane were obtained from Acros. Distilled deionized water was used for the preparation of aqueous solutions. All the chemicals were used as received.

B. Synthesis of Fe_2O_3 MNPs

Spherical Fe_2O_3 MNPs were prepared through a modified thermal decomposition method first developed by Colvin and his coworkers [33]. As shown in the schematic diagram in Fig. 1, FeOOH fine powder (2 mmol), oleic acid (8 mmol), and octadecene (10 ml) were added into a three-neck flask equipped with thermal-couple probe, heating mantle, and Allihn condenser. The mixture was vigorously stirred under a flow of nitrogen, and first heated to 200 °C for 30 min, and then heated to 300 °C for 1 h. Finally, the resulting solution was cooled to room temperature by removing the heat source. The solution was purified by adding chloroform and acetone at a volume ratio of 1:3 and a black precipitate was obtained *via* centrifugation. The purification operation was repeated for two times. Finally the precipitated product was redispersed in 6 ml chloroform for further use. By changing the amount of octadecene and altering the molar ratio of FeOOH to oleic acid, Fe_2O_3 MNPs with diameters ranging from 10 nm to 20 nm were obtained.

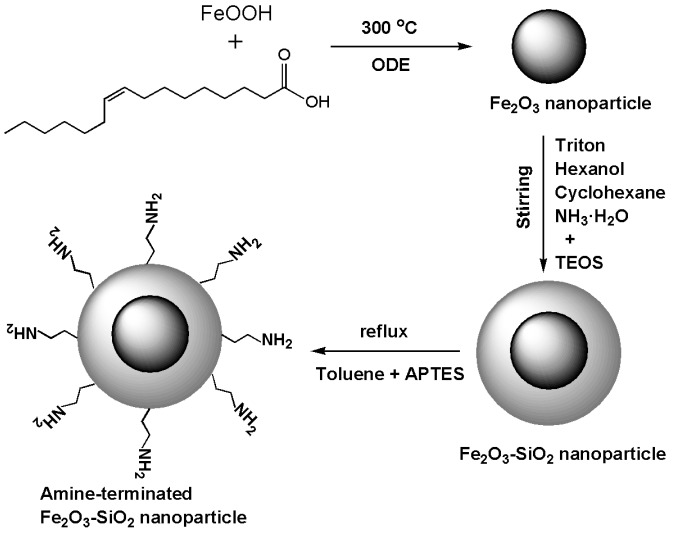

Fig. 1. Schematic diagram for the synthesis of amine-functionalized core-shell Fe_2O_3-SiO_2 MNPs.

C. Synthesis of Fe_2O_3-SiO_2 MNPs

Core-shell Fe_2O_3-SiO_2 MNPs were produced through the formation of reverse microemulsion [34]. At first, Fe_2O_3 MNP was dried in vacuum and dissolved in cyclohexane at a concentration of 0.2 mg/ml. As illustrated in Fig. 1, Triton-X100 (1.79 g), hexanol (1.6 ml), water (393 ul), and aqueous ammonia (107 ul) were added into 8.89 ml cyclohexane of MNPs to form an optimized inverse microemulsion system after being stirred at room temperature for 14 h. Subsequently, TEOS (25 ul) was added dropwise, and the mixture was continuously stirred for 2 h at room temperature. The Fe_2O_3-SiO_2 MNPs were precipitated by adding excess ethanol through centrifugation. Finally, the precipitated products were redispersed in 6 ml ethanol. By changing the Fe_2O_3 MNP concentration and the TEOS reaction time, shell thickness of the Fe_2O_3-SiO_2 MNPs was adjusted from 9 nm to 18 nm.

D. Preparation of Amine-Functionalized Fe_2O_3-SiO_2 MNPs

Amine functionalized Fe_2O_3-SiO_2 MNPs were prepared through a protocol described by Philipse and Vrij [35]. As schematically presented in Fig. 1, surface functionalization of Fe_2O_3-SiO_2 MNPs was carried out through the silanization of aminosilane. The as-synthesized Fe_2O_3-SiO_2 MNPs (4 mg) were dried and dispersed in toluene (6 ml) by stirring for 10 min. By adding APTES (80 ul), the mixture was first heated to 100 °C for 20 min, and then refluxed for 10 h under nitrogen. Afterwards, the solution was centrifuged and the precipitates were washed with toluene for several times. Finally, amine functionalized Fe_2O_3-SiO_2 MNPs were dispersed in 3 ml anhydrous toluene.

E. Immobilization of Amine-Functionalized MNPs

Au surface was prepared by depositing a 20-nm layer of gold onto silicon substrate *via* sputter coating. As illustrated in Fig. 2, nanoparticle immobilization was performed by directly immersing the gold coated silicon substrate into the toluene solution containing amine functionalized Fe_2O_3-SiO_2 MNPs. The functionalized nanoparticles were adsorbed on the gold surface through the charge-neutral amine/gold interactions [36]–[43]. After immobilization for 1 h, the substrate was

This article has been accepted for publication in a future issue of this journal, but has not been fully edited. Content may change prior to final publication. Citation information: DOI 10.1109/TNANO.2016.2636254, IEEE Transactions on Nanotechnology

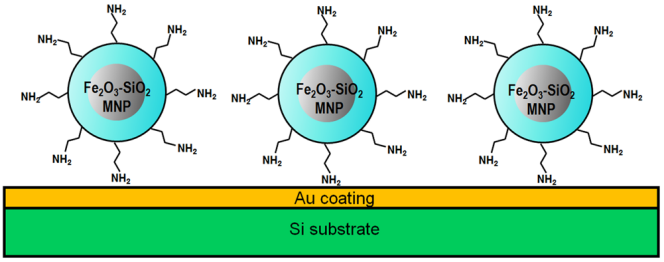

Fig. 2. Schematic illustration of the immobilization of amine-functionalized Fe_2O_3-SiO_2 MNPs on Au surface.

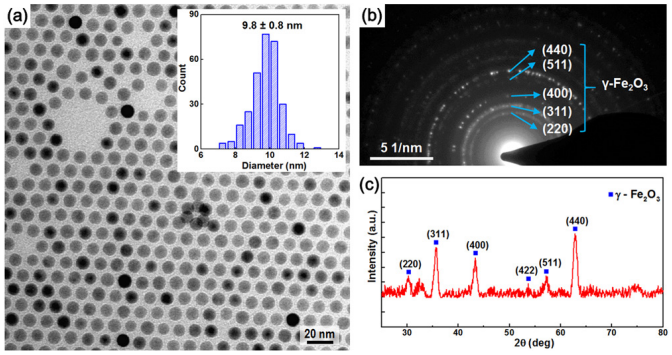

Fig. 3. (a) TEM image (inset: histogram of particle size), (b) SAED patterns and (c) XRD patterns of Fe_2O_3 MNPs.

rinsed several times using pure toluene to remove residual materials and then allowed to dry in ambient environment.

F. Characterization

The morphologies of the nanoparticles were characterized using a Philips CM-100 transmission electron microscope (TEM) operated at 100 kV. The structures of the nanoparticles were characterized by high-resolution TEM and selected area electron diffraction (SAED) on an FEI tecnai-G2 TEM operated at 200 kV. The X-ray powder diffraction patterns of the nanoparticles were collected on a Bruker D8-Advance X-ray diffractometer with Cu Kα radiation (λ = 1.5418 Å). The Fourier transform infrared (FTIR) spectra of the nanoparticles were obtained by a Shimadzu FTIR-8300 spectrometer. The thermal gravimetric analysis (TGA) of the nanoparticles was performed using a TA-Q50 TGA operated at a heating rate of 10 ºC/min from 40 ºC to 500 ºC under N_2. The temperature dependent magnetization curves of the nanoparticles (5 mg) were measured using a Cryogenic vibrating sample magnetometer (VSM). In the zero-field-cooled (ZFC) measurement, the sample was cooled to 50 K without applied field, and then the magnetization was recorded under an applied field of 200 Oe as the temperature increased. In the field-cooled (FC) measurement, an applied field of 200 Oe was applied during sample cooling and magnetization recording. The field dependent magnetization curves of the nanoparticles were obtained by measuring their hysteresis loops using a MicroSense VSM at 300 K. The surface morphologies and elemental compositions of the nanoparticles adsorbed on Au surface were analyzed using an Olympus BX-51 optical microscope and a LEO 1530 scanning electron microscope (SEM).

III. Results and Discussion

A. Characterization of Iron Oxide MNPs and Their Particle Size Control

Fe_2O_3 MNPs with appropriate surface chemistry have been widely used for biomedical and biochemistry applications, due to their high saturation magnetization and small coercivity [1]. Additionally, their magnetic properties are strongly dependent on the particle size [1]. Herein, the as-synthesized Fe_2O_3 MNPs were characterized and their size tuning was investigated.

The morphology of the Fe_2O_3 MNPs is shown in the TEM micrograph in Fig. 3(a), and the particles are in spherical shape, forming a well-ordered monolayer. Histogram of particle size in the inset reveals that the Fe_2O_3 MNPs are monodisperse with a size distribution of 8 % and a diameter of 9.8 ± 0.8 nm. Electron diffraction patterns in Fig. 3(b) show five distinct diffraction rings and their measured lattice spacing can be well indexed to the major *d*-spacing of γ-Fe_2O_3 (JCPDF #04-0755). Crystal structures of the Fe_2O_3 MNPs were identified by XRD, as shown in Fig. 3(c). The positions of all the six diffraction peaks match well with standard powder diffraction data of magnetite with inverse spinel structure.

The monodisperse Fe_2O_3 MNPs were synthesized through thermal decomposition method [33], [44]. The intermediate heating stage at 200 ºC ensures that the inorganic FeOOH precursor was well dissolved in the organic solvent, forming iron carboxylate salt [6]. The final heating stage at 300 ºC resulted in the pyrolysis of iron carboxylate salt and the formation of iron oxide nanocrystals [6]. Octadecene was used as the organic solvent due to its high boiling point as well as its non-polar and non-coordinating properties, favoring the isotropic growth of nanocrystals at elevated temperature [44]. Oleic acid was used as the capping agent for Fe_2O_3 MNPs, due to the strong affinity between its carboxylic group and the surface atoms of Fe_2O_3 MNPs. Besides, the long-chain oleic acid serving as surfactant also provides the Fe_2O_3 MNPs with excellent solubility in non-polar organic solvent, such as hexane, toluene, and chloroform.

The particle size of Fe_2O_3 MNPs is one of the most critical parameters influencing their magnetic properties [45]. Some literature and experimental evidence indicate that factors such as precursor, surfactant, and organic solvent play important roles in determining the size of Fe_2O_3 MNPs [6]. Herein, by altering the ratio of surfactant to precursor and changing the amount of organic solvent, the size of Fe_2O_3 MNPs was tuned from 10 nm to 20 nm, as shown in the TEM images in Fig. 4. When the molar ratio of surfactant to precursor was changed from 4:1 to 6:1 and the amount of octadecene was kept constant (10 ml), the particle size slightly increased from 10 nm to 12 nm, as shown in Fig. 4(a) and Fig. 4(b). When the ratio of surfactant to precursor was kept constant at 4:1 and the amount of octadecene was increased from 10 ml to 20 ml, the particle size significantly increased from 12 nm to 20 nm, as shown in Fig. 4(b) and Fig. 4(c). The size tuning of the Fe_2O_3 MNPs can

This article has been accepted for publication in a future issue of this journal, but has not been fully edited. Content may change prior to final publication. Citation information: DOI 10.1109/TNANO.2016.2636254, IEEE Transactions on Nanotechnology

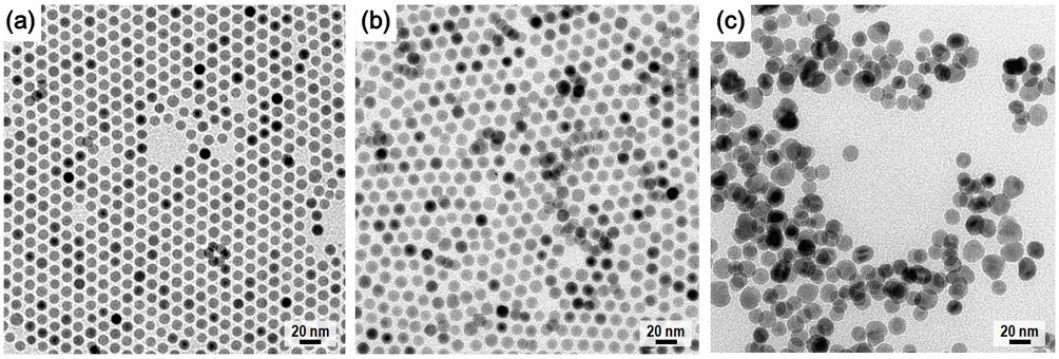

Fig. 4. TEM images of (a) 10 nm, (b) 12 nm, and (c) 20 nm Fe_2O_3 MNPs.

be explained by that excess surfactant probably inhibit the formation of iron oxide nuclei [6], producing fewer nanocrystals with larger size. On the other hand, increasing the solvent amount reduces the concentration of iron oxide nuclei, and this may elevate the nucleation threshold, leading to fewer nuclei and hence larger nanoparticles [46]. Above all, our results suggest that the molar ratio of surfactant to precursor and the amount of organic solvent both have influence on the particle size of Fe_2O_3 MNPs.

B. Silica Coating of MNPs and Their Shell Thickness Control

To transfer the Fe_2O_3 MNPs from organic phase to aqueous media, surface modification is required. Silica coating is a very promising surface modifier due to its excellent biocompatibility and facile conjugation with various functional groups [14]. The shell thickness of the silica coated Fe_2O_3 MNPs greatly affects their individual and collective magnetic properties. In this regard, core-shell Fe_2O_3-SiO_2 MNPs were synthesized and the thickness control of their silica shells was investigated. The as-synthesized Fe_2O_3 MNPs were used as the magnetic cores for the chemical synthesis of Fe_2O_3-SiO_2 MNPs *via* reverse microemulsion method. A representative TEM image of the Fe_2O_3-SiO_2 MNPs was shown in Fig. 5(a). It is observed that the particle is composed of spherical magnetic core with 10 nm diameter and silica shell with 9 nm thickness. High-resolution TEM image in the inset of Fig. 5(a) shows that the light-colored shell is amorphous, whereas the dark-colored core is highly crystalline with a lattice fringe of 0.251 nm, corresponding to the (311) plane of γ-Fe_2O_3. The high-resolution TEM result confirms that the spherical iron oxide core is capped by a uniform layer of silica coating.

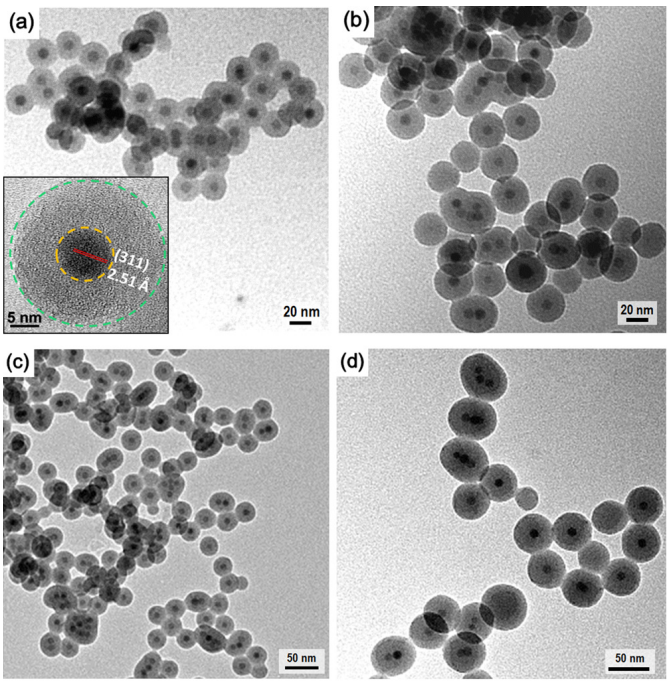

Fig. 5. TEM images of Fe_2O_3-SiO_2 MNPs: (a) 10 nm core diameter and 9 nm shell thickness; (b) 10 nm core diameter and 13 nm shell thickness; (c) 10 nm core diameter and 11 nm shell thickness; (d) 10 nm core diameter and 18 nm shell thickness. Inset: high-resolution TEM images revealing the structure and crystallinity of the core-shell MNP.

The formation mechanism of the silica coating on Fe_2O_3 MNPs is mainly related to the phase transfer of the Fe_2O_3-SiO_2 MNPs from organic phase to aqueous phase. At first, an inverse microemulsion system consisting of water, oil, and surfactant were formed. Subsequently, the TEOS added into this system underwent hydrolysis reaction and exchanged with the hydrophobic ligands on the Fe_2O_3 MNPs, which were transferred from organic phase into aqueous phase [34], [47]. The inverse micelles and the continuously hydrolyzed TEOS resulted in the condensation and growth of amorphous silica on the surface of phase-transferred MNPs [34], [48].

Fe_2O_3-SiO_2 MNPs with different shell thickness exhibit distinct properties, including surface-to-volume ratio, effective magnetization, and dipole interactions, and thus it is necessary to control the shell thickness as desired. To investigate the influence of Fe_2O_3 MNP concentration on the shell thickness, the concentration of Fe_2O_3 MNP solution was decreased from 0.2 mg/ml to 0.125 mg/ml, while other parameters were unchanged and the TEOS reaction time was kept at 2 h. As a result, the silica coating was increased from 9 nm to 13 nm, as presented in Fig. 5(a) and Fig. 5(b). To investigate the influence of reaction time on the shell thickness, the TEOS reaction time was increased from 2 h to 5 h, while the Fe_2O_3 MNP concentration was kept at 0.2 mg/ml. This led to the slight increase of the shell thickness from 9 nm to 11 nm, as presented in Fig. 5(a) and Fig. 5(c). Additionally, when the Fe_2O_3 MNP

This article has been accepted for publication in a future issue of this journal, but has not been fully edited. Content may change prior to final publication. Citation information: DOI 10.1109/TNANO.2016.2636254, IEEE Transactions on Nanotechnology

concentration was 0.125 mg/ml, by elongating the TEOS reaction time from 2 h to 5 h, the shell thickness was notably increased from 13 nm to 18 nm, as presented in Fig. 5(b) and Fig. 5(d). Based on our experimental results, it can be inferred that a relatively low level of Fe_2O_3 MNP concentration enhances the growing rate of silica shell. Besides, by increasing the TEOS reaction time, more ligands can be exchanged and attached on the surface of MNPs, promoting the growth of the silica shell. Such effect would become more pronounced when the Fe_2O_3 MNP concentration is low. As a short summary, the regulation of the silica shell thickness of Fe_2O_3-SiO_2 MNPs can be achieved by altering the concentration of Fe_2O_3 MNPs or the reaction time of TEOS.

C. *Amine Functionalization of Core-Shell MNPs*

The Fe_2O_3-SiO_2 MNPs could be further functionalized with amine-terminated APTES to fulfill the tasks of conjugation and immobilization [12], [21]. Here, Fe_2O_3-SiO_2 MNPs with 10 nm core diameter and 9 nm shell thickness were used for amine functionalization. The morphology of the functionalized MNPs was shown in the TEM images in Fig. 6(a) and Fig. 6(b). It is observed that most of the particles are spherical and separated, and their core-shell structures are well retained.

The amine functionalization of the Fe_2O_3-SiO_2 MNPs was achieved using amine-terminated silanes (APTES) through silanization process. In this process, the surface of Fe_2O_3-SiO_2 MNPs were chemically modified with amine groups using APTES under anhydrous conditions. At first, APTES was absorbed on the silica surface through hydrogen bonds, which was formed between the amine group of APTES and the silanol group on silica [49]. Proton transfer occurred in some of the formed hydrogen bonds, resulting in stronger ionic interactions [49]. At elevated temperature, the condensation reaction between the APTES and the silanol molecules on silica surface proceeded [50], [51]. This led to the formation of Si–O–Si covalent bond, with the amine group of APTES being expelled from silica surface [52]. Finally the amine-terminated ligands were grafted on the silica surface of the core-shell MNPs.

The amine groups on the functionalized Fe_2O_3-SiO_2 MNPs were qualitatively confirmed by FTIR, as shown in Fig. 7(a). The intensive bands at 1033 cm^{-1} represent the asymmetric stretching and bending of siloxane groups (Si–O–Si). The

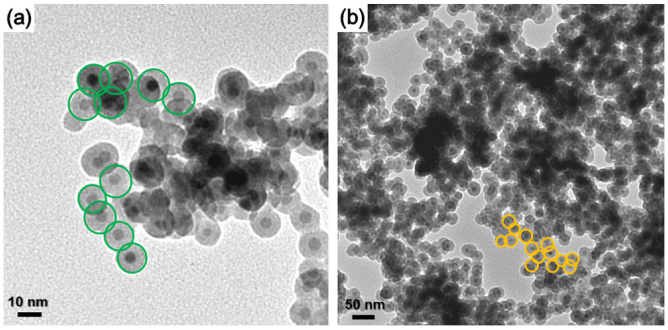

Fig. 6. (a) High magnification and (b) low magnification TEM images of amine-functionalized Fe_2O_3-SiO_2 MNPs (10 nm core diameter, 9 nm shell thickness). Representative nanoparticles are delineated by colored circles.

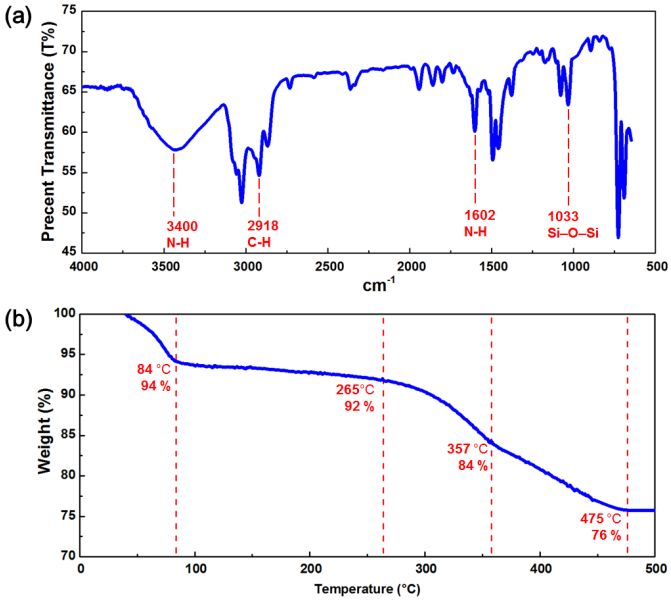

Fig. 7. (a) FTIR spectrum and (b) TGA curve of amine-functionalized Fe_2O_3-SiO_2 MNPs.

absorption bands near 3400 cm^{-1} and 1602 cm^{-1} represent the stretching and bending vibrations of N–H, indicating the existence of amine groups. The band at 3400 cm^{-1} is also related to the overlapping of N–H vibration with silanol stretching [53]. The weak band at 2918 cm^{-1} in the region of 2850–2950 cm^{-1} is ascribed to the C–H stretching from the propyl chain of APTES [54]. The C–N stretching vibration normally appears in the range of 1000–1200 cm^{-1} [55]. However, this peak was not resolved here probably due to its overlay with the IR absorptions of Si–O–Si in the range of 1130–1000 cm^{-1} and the IR absorptions of Si–CH_2–R in the range of 1250–1200 cm^{-1} [56].

To quantify the average number of amine groups on each functionalized Fe_2O_3-SiO_2 MNP, the mass decrease of the sample upon heating was investigated by TGA, as presented in Fig. 7(b). Initially, the sample shows a weight loss of 6% from 40 °C to 84 °C, which is attributed to the evaporation of volatile solvent (toluene). The cumulative weight loss of 8% from 265 °C to 357 °C may result from desorption of the APTES (boiling point: 217 °C) from the surface of the core-shell MNPs. The final weight loss of 8% from 357 °C to 475 °C can be related to desorption of the oleic acid (boiling point: 360 °C). The TGA curve indicates that the content of Fe_2O_3-SiO_2 is 76 wt% and the content of APTES is 8 wt% in our sample. Based on the TGA results, the size (core diameter: 10 nm, shell thickness: 9 nm) and the density (γ-Fe_2O_3: 4.87 g/cm^3, amorphous SiO_2: 2.20 g/cm^3) of a core-shell MNP, and also the molar mass of APTES (221.37 g/mol), the average number of amine groups on each functionalized Fe_2O_3-SiO_2 MNP is estimated to be 7.6×10^3.

D. *Magnetic Properties of MNPs*

The temperature dependent magnetization (ZFC/FC curves) of the Fe_2O_3 MNPs were recorded using VSM, as shown in Fig. 8(a). In the ZFC curve, the maximum of the magnetization

This article has been accepted for publication in a future issue of this journal, but has not been fully edited. Content may change prior to final publication. Citation information: DOI 10.1109/TNANO.2016.2636254, IEEE Transactions on Nanotechnology

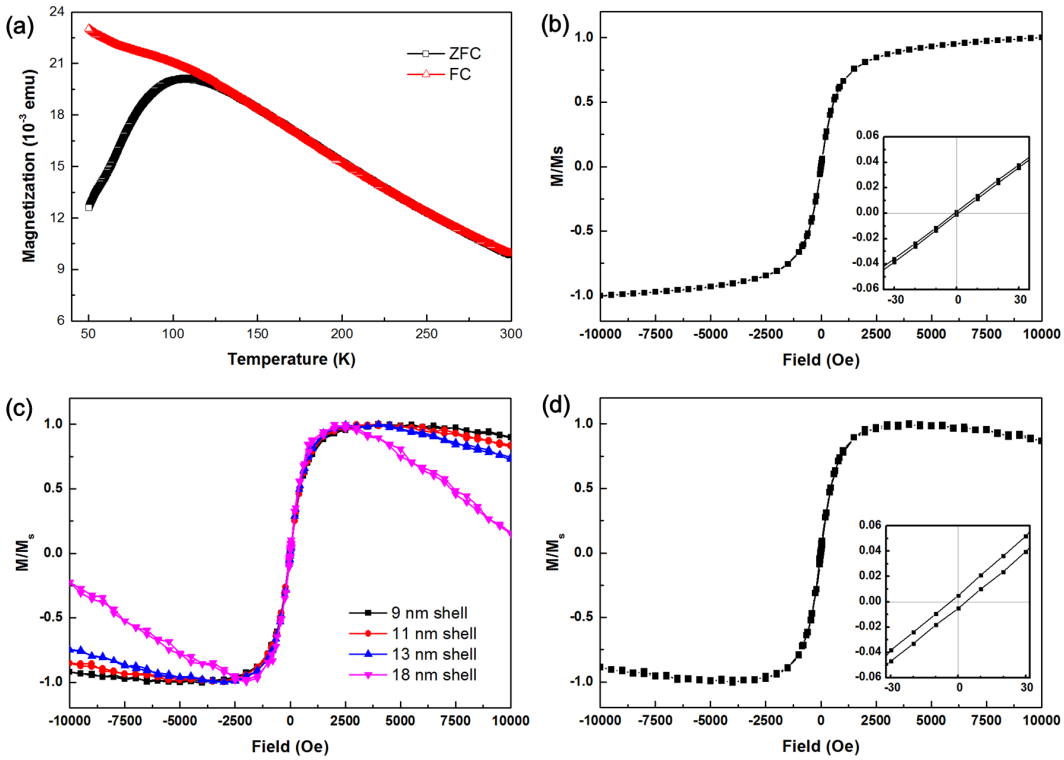

Fig. 8. (a) ZFC and FC curves of 10 nm Fe_2O_3 MNPs. MH curves at 300 K of (b) 10 nm Fe_2O_3 MNPs, (c) Fe_2O_3-SiO_2 MNPs with the same core diameter (10 nm) but different shell thickness (9 nm, 11 nm, 13 nm, and 18 nm), and (d) amine functionalized Fe_2O_3-SiO_2 MNPs (10 nm core diameter, 9 nm shell thickness). Inset: the enlarged curves near the origin.

corresponds to the blocking temperature (T_B), which is defined as the temperature at which the nanoparticle moments do not relax during the time scale of the measurement [57]. Using the blocking temperature, the magnetic anisotropy energy constant K_{eff} of the nanoparticle at a typical volume V (determined from TEM) can be calculated through the relation: $K_{eff} = 25k_BT_B/V$, where k_B is the Boltzmann constant [45]. For our 10 nm Fe_2O_3 nanoparticles, the measured blocking temperature is equal to 105 K, and the corresponding anisotropy constant K_{eff} is estimated to be 6.9×10^5 erg/cm^3, which is close to the K_{eff} of iron oxide nanoparticles (4.5×10^5 erg/cm^3) reported in other study [57]. The estimated K_{eff} of our Fe_2O_3 nanoparticles is larger than the first-order magnetocrystalline anisotropy value of the bulk maghemite (0.5×10^5 erg/cm^3), and such enhancement is presumably associated with the surface anisotropy contribution from the nanoparticles [45].

The field dependent magnetization (MH curves) of the Fe_2O_3 MNPs before silica coating, after silica coating, and after amine functionalization were measured using VSM respectively. Fig. 8(b) shows the hysteresis loop of the as-synthesized 10 nm Fe_2O_3 MNPs, and a small coercivity H_c of 0.88 Oe was measured. The MH curve reveals that the Fe_2O_3 MNPs almost retain no magnetization at room temperature, when there is no external field. The black curve in Fig. 8(c) shows the hysteresis loop of the Fe_2O_3-SiO_2 MNPs with 10 nm core diameter and 9 nm shell thickness, and the measured coercivity H_c was 5.5 Oe. It is noteworthy that the hysteresis curve demonstrates diamagnetic behavior at high magnetic field (>2 kOe) due to the diamagnetic contribution from the silica shell. Fig. 8(d) shows the hysteresis loop of the amine functionalized Fe_2O_3-SiO_2 MNPs (10 nm core diameter, 9 nm shell thickness), with the coercivity H_c being 2.5 Oe. This curve is similar to that of the Fe_2O_3-SiO_2 MNPs without amine functionalization, considering the fact that the core-shell structures are the same among these two types of MNPs. Additionally, coercivity changes of the MNPs were observed after silica coating and after functionalization, and this presumably originates from the change of the surface states of the magnetic core and the silica shell. Further investigation will be carried out for the MNPs to correlate their surface properties with their magnetic properties.

The MH curves of the core-shell Fe_2O_3-SiO_2 MNPs with the same core diameter (10 nm) but different shell thickness (9 nm, 11 nm, 13 nm, 18 nm) were measured and compared, as shown in the four curves with different colors in Fig. 8(c). It is observed that when the thickness of the silica shell on the Fe_2O_3 core is increased, the diamagnetic behavior at high magnetic field become more significant and the magnetization tend to decrease. This could be explained by the fact that the nearly superparamagnetic contribution from the iron oxide core is compromised by the diamagnetic contribution from the silica shell, especially at high magnetic field. Additionally, magnetic dipole interactions between adjacent Fe_2O_3-SiO_2 MNPs become less pronounced, when the thickness of the silica shell is increased and the inter-particle distance is decreased correspondingly.

This article has been accepted for publication in a future issue of this journal, but has not been fully edited. Content may change prior to final publication. Citation information: DOI 10.1109/TNANO.2016.2636254, IEEE Transactions on Nanotechnology

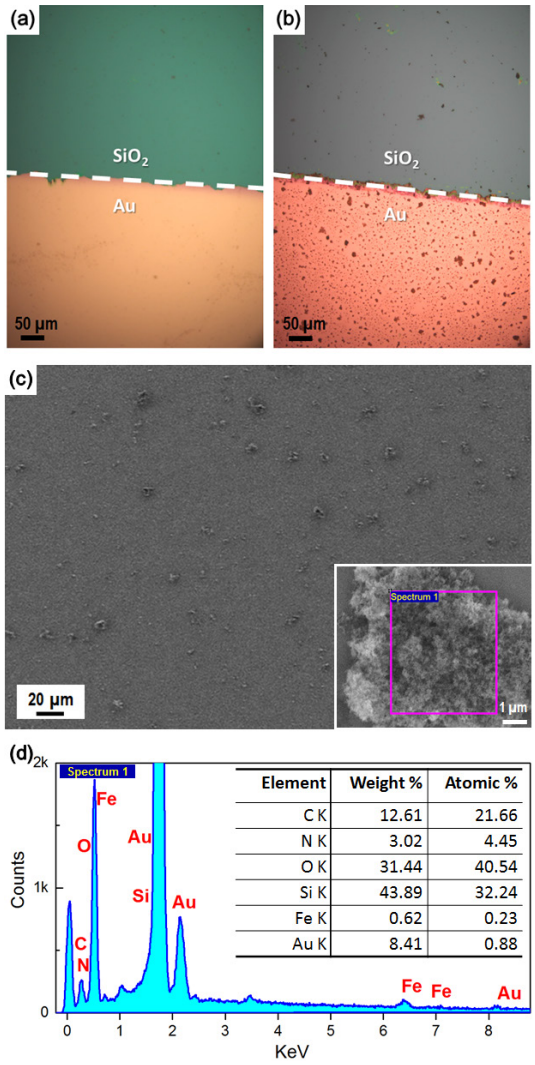

Fig. 9. Optical images of Si substrate partially coated by Au (a) before and (b) after immobilization of amine functionalized Fe_2O_3-SiO_2 MNPs; (c) SEM image (inset: the enlarged image) and (d) EDX and elemental analysis of the nanoparticles adsorbed on Au surface.

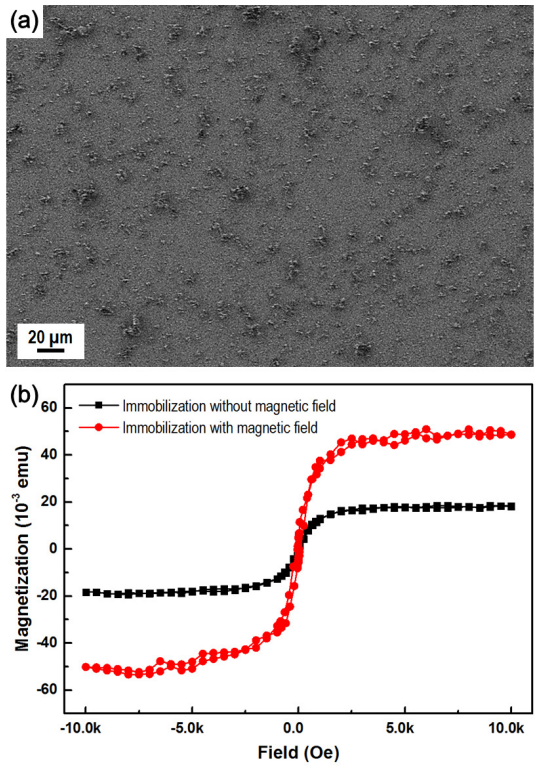

Fig. 10. (a) SEM image of the amine functionalized Fe_2O_3-SiO_2 MNPs adsorbed on Au surface in the presence of applied magnetic field. (b) hysteresis loops of the sample in Fig. 9c (nanoparticles immobilized under no magnetic field) and the sample in Fig. 10a (nanoparticles immobilized under magnetic field).

E. Immobilization of Amine-Functionalized MNPs

As shown in the optical micrograph in Fig. 9(a), silicon wafer with partially coated gold surface was used as the substrate for the immobilization test of amine-functionalized MNPs. It has been theoretically and experimentally reported that amine with lone-pair electrons could adsorb onto zero-valent Au surface through electronic coupling [36]–[39]. It is noteworthy that the binding energy of the amines on gold surface is much weaker than that for thiols [40], [41]. Besides, low-polarity solvent is preferred for dispersing the amines in order to reduce the influence of solvent interactions on amine/gold interactions [42], [43]. Considering this, toluene solution containing the amine-terminated Fe_2O_3-SiO_2 MNPs was used for nanoparticle immobilization. The surface morphology of the sample is shown in the optical micrograph in Fig. 9(b). Multiple dots with relatively uniform distribution were selectively adsorbed on the gold surface but not on the silicon substrate. SEM micrograph of the adsorbed substances is presented in Fig. 9(c). It is observed that the micron-sized dots are composed of assembled nanoparticles and they were attached on the substrate surface. The EDX spectrum and elemental analysis of the adsorbed nanoparticles are presented in Fig. 9(d). Herein, the Fe peak was produced from the Fe_2O_3 core, the Si peak was originated from both the silica shell and the silicon substrate, the N peak was generated from the amine groups capped on the surface of MNPs, the Au peak was attributed to the gold surface, and the C peak as well as the O peak were related to the organic substances. The results of elemental analysis confirm the existence of amine, silica, and iron oxide in the functionalized core-shell MNPs.

The influence of external magnetic field on the immobilization process was investigated. The sample was prepared by immersing the gold coated silicon substrate onto the nanoparticle solution under an out-of-plane magnetic field (magnitude: 300 Oe, gradient: 30 Oe/mm) for 1 h. As shown in the SEM micrograph in Fig. 10(a), the magnetically immobilized MNPs were adsorbed on the gold surface in a relatively high density. Moreover, the hysteresis loops in Fig. 10(b) reveal that the saturation magnetization value (5×10^{-2} emu) of the magnetically immobilized sample is larger than that (2×10^{-2} emu) of the control sample, which was obtained under no applied magnetic field. The higher density of the adsorbed MNPs and the larger saturation magnetization observed in the magnetically immobilized sample suggest that the

immobilization process was enhanced when external magnetic field was introduced. Such enhancement is presumably related to the aggregation and assembly of the MNPs under the guidance of applied magnetic field, which may facilitate the interactions between the amine group on nanoparticle surface and the gold surface of the substrate. Future work will be carried out to functionalize the gold surface with carboxyl groups for the purpose of achieving more stable and reliable immobilization of the amine-terminated MNPs on carboxyl-terminated Au surface through NH_2-COOH binding.

IV. Conclusion

An effective and facile protocol was developed for chemically synthesizing amine terminated core-shell Fe_2O_3-SiO_2 MNPs. The core diameter and shell thickness of the Fe_2O_3-SiO_2 MNPs were tuned and controlled by changing experimental parameters. By increasing the silica coating thickness in the core-shell MNPs, the decline of their magnetization at high magnetic field became more pronounced. The functionalized core-shell MNPs were adsorbed on gold surface due to the charge-neutral amine/gold interactions. Such immobilization process was observed to be enhanced under external magnetic field. The functionalized core-shell MNPs can be further conjugated with other biomolecules, enabling their biomedical applications.

V. Acknowledgment

This research was supported by the Seed Funding Program for Basic Research, Seed Funding Program for Applied Research and Small Project Funding Program from University of Hong Kong, ITF Tier 3 funding (ITS-104/13, ITS-214/14), and University Grants Committee of HK (AoE/P-04/08).

References

[1] A. K. Gupta, and M. Gupta, "Synthesis and surface engineering of iron oxide nanoparticles for biomedical applications," *Biomaterials,* vol. 26, no. 18, pp. 3995–4021, 2005.

[2] N. Lee, D. Yoo, D. Ling, M. H. Cho, T. Hyeon, and J. Cheon, "Iron oxide based nanoparticles for multimodal imaging and magnetoresponsive therapy," *Chem. Rev.,* vol. 115, no. 19, pp. 10637–10689, 2015.

[3] P. Kucheryavy, J. He, V. T. John, P. Maharjan, L. Spinu, G. Z. Goloverda, and V. L. Kolesnichenko, "Superparamagnetic iron oxide nanoparticles with variable size and an iron oxidation state as prospective imaging agents," *Langmuir,* vol. 29, no. 2, pp. 710–716, 2013.

[4] P. Guardia, A. Labarta, and X. Batlle, "Tuning the size, the shape, and the magnetic properties of iron oxide nanoparticles," *J. Phys. Chem. C,* vol. 115, no. 2, pp. 390–396, 2010.

[5] P. Velusamy, S. Chia-Hung, A. Shritama, G. V. Kumar, V. Jeyanthi, and K. Pandian, "Synthesis of oleic acid coated iron oxide nanoparticles and its role in anti-biofilm activity against clinical isolates of bacterial pathogens," *J. Taiwan Inst. Chem. Eng.,* vol. 59, pp. 450–456, 2016.

[6] W. Y. William, J. C. Falkner, C. T. Yavuz, and V. L. Colvin, "Synthesis of monodisperse iron oxide nanocrystals by thermal decomposition of iron carboxylate salts," *Chem. Commun.*, no. 20, pp. 2306–2307, 2004.

[7] J. Park, K. An, Y. Hwang, J.-G. Park, H.-J. Noh, J.-Y. Kim, J.-H. Park, N.-M. Hwang, and T. Hyeon, "Ultra-large-scale syntheses of monodisperse nanocrystals," *Nat. Mater.,* vol. 3, no. 12, pp. 891–895, 2004.

[8] T. Hyeon, S. S. Lee, J. Park, Y. Chung, and H. B. Na, "Synthesis of highly crystalline and monodisperse maghemite nanocrystallites without a size-selection process," *J. Am. Chem. Soc.,* vol. 123, no. 51, pp. 12798–12801, 2001.

[9] J. Rockenberger, E. C. Scher, and A. P. Alivisatos, "A new nonhydrolytic single-precursor approach to surfactant-capped nanocrystals of transition metal oxides," *J. Am. Chem. Soc.,* vol. 121, no. 49, pp. 11595–11596, 1999.

[10] S. Sun, and H. Zeng, "Size-controlled synthesis of magnetite nanoparticles," *J. Am. Chem. Soc.,* vol. 124, no. 28, pp. 8204–8205, 2002.

[11] T.-Q. Nguyen, J. Wu, V. Doan, B. J. Schwartz, and S. H. Tolbert, "Control of energy transfer in oriented conjugated polymer-mesoporous silica composites," *Science,* vol. 288, no. 5466, pp. 652–656, 2000.

[12] V. Maurice, C. Slostowski, N. Herlin-Boime, and G. Carrot, "Polymer-Grafted Silicon Nanoparticles Obtained Either via Peptide Bonding or Click Chemistry," *Macromol. Chem. Phys.,* vol. 213, no. 23, pp. 2498–2503, 2012.

[13] D. K. Yi, S. S. Lee, G. C. Papaefthymiou, and J. Y. Ying, "Nanoparticle architectures templated by SiO_2/Fe_2O_3 nanocomposites," *Chem. Mater.,* vol. 18, no. 3, pp. 614–619, 2006.

[14] H. Ding, Y. Zhang, S. Wang, J. Xu, S. Xu, and G. Li, "Fe_3O_4@ SiO2 core/shell nanoparticles: the silica coating regulations with a single core for different core sizes and shell thicknesses," *Chem. Mater.,* vol. 24, no. 23, pp. 4572–4580, 2012.

[15] S. Santra, R. Tapec, N. Theodoropoulou, J. Dobson, A. Hebard, and W. Tan, "Synthesis and characterization of silica-coated iron oxide nanoparticles in microemulsion: the effect of nonionic surfactants," *Langmuir,* vol. 17, no. 10, pp. 2900–2906, 2001.

[16] M. Darbandi, R. Thomann, and T. Nann, "Single quantum dots in silica spheres by microemulsion synthesis," *Chem. Mater.,* vol. 17, no. 23, pp. 5720–5725, 2005.

[17] M. Darbandi, W. Lu, J. Fang, and T. Nann, "Silica encapsulation of hydrophobically ligated PbSe nanocrystals," *Langmuir,* vol. 22, no. 9, pp. 4371–4375, 2006.

[18] Y. Li, B. Yan, C. Deng, W. Yu, X. Xu, P. Yang, and X. Zhang, "Efficient on-chip proteolysis system based on functionalized magnetic silica microspheres," *Proteomics,* vol. 7, no. 14, pp. 2330–2339, 2007.

[19] X. Xu, C. Deng, M. Gao, W. Yu, P. Yang, and X. Zhang, "Synthesis of magnetic microspheres with immobilized metal ions for enrichment and direct determination of phosphopeptides by matrix-assisted laser desorption ionization mass spectrometry," *Adv. Mater.,* vol. 18, no. 24, pp. 3289–3293, 2006.

[20] L. Levy, Y. Sahoo, K.-S. Kim, E. J. Bergey, and P. N. Prasad, "Nanochemistry: synthesis and characterization of multifunctional nanoclinics for biological applications," *Chem. Mater.,* vol. 14, no. 9, pp. 3715–3721, 2002.

[21] D. Gao, Z. Zhang, M. Wu, C. Xie, G. Guan, and D. Wang, "A surface functional monomer-directing strategy for highly dense imprinting of TNT at surface of silica nanoparticles," *J. Am. Chem. Soc.,* vol. 129, no. 25, pp. 7859–7866, 2007.

[22] N. García, E. Benito, J. Guzmán, P. Tiemblo, V. Morales, and R. A. García, "Functionalization of SBA-15 by an acid-catalyzed approach: A surface characterization study," *Microporous Mesoporous Mater.,* vol. 106, no. 1, pp. 129–139, 2007.

[23] E. Battistel, and D. Bianchi, "Thermodynamics of immobilized ribonuclease A," *Pure Appl. Chem.,* vol. 63, no. 10, pp. 1483–1490, 1991.

[24] M. C. Burleigh, M. A. Markowitz, M. S. Spector, and B. P. Gaber, "Direct synthesis of periodic mesoporous organosilicas: functional incorporation by co-condensation with organosilanes," *J. Phys. Chem. B,* vol. 105, no. 41, pp. 9935–9942, 2001.

[25] Q. Wei, Z.-R. Nie, Y.-L. Hao, L. Liu, Z.-X. Chen, and J.-X. Zou, "Effect of synthesis conditions on the mesoscopical order of mesoporous silica SBA-15 functionalized by amino groups," *J. Sol-Gel Sci. Technol.,* vol. 39, no. 2, pp. 103–109, 2006.

[26] S. L. Burkett, S. D. Sims, and S. Mann, "Synthesis of hybrid inorganic–organic mesoporous silica by co-condensation of siloxane and organosiloxane precursors," *Chem. Commun.*, no. 11, pp. 1367–1368, 1996.

[27] L. Mercier, and T. J. Pinnavaia, "Direct synthesis of hybrid organic-inorganic nanoporous silica by a neutral amine assembly route: structure-function control by stoichiometric incorporation of

organosiloxane molecules," *Chem. Mater.,* vol. 12, no. 1, pp. 188–196, 2000.

[28] Z.-H. Wang, and G. Jin, "Silicon surface modification with a mixed silanes layer to immobilize proteins for biosensor with imaging ellipsometry," *Colloids Surf., B,* vol. 34, no. 3, pp. 173–177, 2004.

[29] D. K. Yi, S. T. Selvan, S. S. Lee, G. C. Papaefthymiou, D. Kundaliya, and J. Y. Ying, "Silica-coated nanocomposites of magnetic nanoparticles and quantum dots," *J. Am. Chem. Soc.,* vol. 127, no. 14, pp. 4990–4991, 2005.

[30] A. G. Roca, J. F. Marco, M. d. P. Morales, and C. J. Serna, "Effect of nature and particle size on properties of uniform magnetite and maghemite nanoparticles," *J. Phys. Chem. C,* vol. 111, no. 50, pp. 18577–18584, 2007.

[31] M. Zhang, B. L. Cushing, and C. J. O'Connor, "Synthesis and characterization of monodisperse ultra-thin silica-coated magnetic nanoparticles," *Nanotechnology,* vol. 19, no. 8, pp. 085601, 2008.

[32] D. C. Lee, F. V. Mikulec, J. M. Pelaez, B. Koo, and B. A. Korgel, "Synthesis and magnetic properties of silica-coated FePt nanocrystals," *J. Phys. Chem. B,* vol. 110, no. 23, pp. 11160–11166, 2006.

[33] C. Augustyn, T. Allston, R. Hailstone, and K. Reed, "One-Vessel synthesis of iron oxide nanoparticles prepared in non-polar solvent," *RSC Adv.,* vol. 4, no. 10, pp. 5228–5235, 2014.

[34] C. Vogt, M. S. Toprak, M. Muhammed, S. Laurent, J.-L. Bridot, and R. N. Müller, "High quality and tuneable silica shell–magnetic core nanoparticles," *J. Nanopart. Res.,* vol. 12, no. 4, pp. 1137–1147, 2010.

[35] A. Philipse, and A. Vrij, "Preparation and properties of nonaqueous model dispersions of chemically modified, charged silica spheres," *J. Colloid Interface Sci.,* vol. 128, no. 1, pp. 121–136, 1989.

[36] E. de la Llave, R. Clarenc, D. J. Schiffrin, and F. J. Williams, "Organization of alkane amines on a gold surface: Structure, surface dipole, and electron transfer," *J. Phys. Chem. C*, vol. 118, no. 1, pp. 468–475, 2013.

[37] R. C. Hoft, M. J. Ford, A. M. McDonagh, and M. B. Cortie, "Adsorption of amine compounds on the Au (111) surface: a density functional study," *J. Phys. Chem. C*, vol. 111, no. 37, pp. 13886–13891, 2007.

[38] S. Y. Quek, L. Venkataraman, H. J. Choi, S. G. Louie, M. S. Hybertsen, and J. Neaton, "Amine-gold linked single-molecule circuits: experiment and theory," *Nano Lett.*, vol. 7, no. 11, pp. 3477–3482, 2007.

[39] L. Venkataraman, J. E. Klare, I. W. Tam, C. Nuckolls, M. S. Hybertsen, and M. L. Steigerwald, "Single-molecule circuits with well-defined molecular conductance," *Nano Lett.*, vol. 6, no. 3, pp. 458–462, 2006.

[40] M. B. Haddada, J. Blanchard, S. Casale, J.-M. Krafft, A. Vallée, C. Méthivier, *et al.*, "Optimizing the immobilization of gold nanoparticles on functionalized silicon surfaces: amine- vs thiol-terminated silane," *Gold Bull.*, vol. 46, no. 4, pp. 335–341, 2013.

[41] T. Sainsbury, T. Ikuno, D. Okawa, D. Pacile, J. M. Frechet, and A. Zettl, "Self-assembly of gold nanoparticles at the surface of amine- and thiol-functionalized boron nitride nanotubes," *J. Phys. Chem. C*, vol. 111, no. 35, pp. 12992–12999, 2007.

[42] A. Kumar, S. Mandal, P. Selvakannan, R. Pasricha, A. Mandale, and M. Sastry, "Investigation into the interaction between surface-bound alkylamines and gold nanoparticles," *Langmuir*, vol. 19, no. 15, pp. 6277–6282, 2003.

[43] D. V. Leff, L. Brandt, and J. R. Heath, "Synthesis and characterization of hydrophobic, organically-soluble gold nanocrystals functionalized with primary amines," *Langmuir*, vol. 12, no. 20, pp. 4723–4730, 1996.

[44] C. Jiang, C. W. Leung, and P. W. Pong, "Magnetic-field-assisted assembly of anisotropic superstructures by iron oxide nanoparticles and their enhanced magnetism," *Nanoscale Res. Lett.,* vol. 11, no. 1, pp. 1–12, 2016.

[45] C.-R. Lin, R.-K. Chiang, J.-S. Wang, and T.-W. Sung, "Magnetic properties of monodisperse iron oxide nanoparticles," *J. Appl. Phys.,* vol. 99, no. 8, pp. 08N710, 2006.

[46] Y. Sun, "Controlled synthesis of colloidal silver nanoparticles in organic solutions: empirical rules for nucleation engineering," *Chem. Soc. Rev.,* vol. 42, no. 7, pp. 2497–2511, 2013.

[47] F. Arriagada, and K. Osseo-Asare, "Controlled hydrolysis of tetraethoxysilane in a nonionic water-in-oil microemulsion: a statistical model of silica nucleation," *Colloids Surf., A,* vol. 154, no. 3, pp. 311–326, 1999.

[48] F. Arriagada, and K. Osseo-Asare, "Synthesis of nanosize silica in a nonionic water-in-oil microemulsion: effects of the water/surfactant molar ratio and ammonia concentration," *J. Colloid Interface Sci.,* vol. 211, no. 2, pp. 210–220, 1999.

[49] E. Vansant, P. V. D. Voort, K. Vrancken, and K. Unger, "Characterization and chemical modification of the silica surface," *J. Chromatogr. A,* vol. 738, no. 2, pp. 313–313, 1996.

[50] S. Sadasivan, D. Khushalani, and S. Mann, "Synthesis and shape modification of organo-functionalised silica nanoparticles with ordered mesostructured interiors," *J. Mater. Chem.,* vol. 13, no. 5, pp. 1023–1029, 2003.

[51] J. Kim, P. Seidler, L. S. Wan, and C. Fill, "Formation, structure, and reactivity of amino-terminated organic films on silicon substrates," *J. Colloid Interface Sci.,* vol. 329, no. 1, pp. 114–119, 2009.

[52] W. G. Y. F. T. Zhaogang, Y. Wensheng, and L. Tiejin, "The surface modification of silica with APTS," *Prog. Chem.*, pp. Z1, 2006.

[53] I. Rahman, M. Jafarzadeh, and C. Sipaut, "Synthesis of organo-functionalized nanosilica via a co-condensation modification using γ-aminopropyltriethoxysilane (APTES)," *Ceram. Int.*, vol. 35, no. 5, pp. 1883–1888, 2009.

[54] H. H. Yiu, P. A. Wright, and N. P. Botting, "Enzyme immobilisation using siliceous mesoporous molecular sieves," *Microporous Mesoporous Mater.,* vol. 44, pp. 763–768, 2001.

[55] D. Evans, "The Systematic Identification of Organic Compounds, (Shriner, RL; Hermann, CKF; Morrill, TC; Curtin, DY; Fuson, RC)," *J. Chem. Educ.*, vol. 76, no. 8, pp. 1069, 1999.

[56] L. D. White, and C. P. Tripp, "Reaction of (3-aminopropyl) dimethylethoxysilane with amine catalysts on silica surfaces," *J. Colloid Interface Sci.,* vol. 232, no. 2, pp. 400–407, 2000.

[57] M. Pauly, B. P. Pichon, A. Demortière, J. Delahaye, C. Leuvrey, G. Pourroy, *et al.*, "Large 2D monolayer assemblies of iron oxide nanocrystals by the Langmuir–Blodgett technique," *Superlattices Microstruct.*, vol. 46, no. 1, pp. 195–204, 2009.